



Distortional Post-Buckling Behavior and Strength of Cold-Formed Steel Columns: How does the Cross-Section Geometry Affect it?

A. Landesmann¹, D. Camotim², C. Basaglia³

Abstract

This paper reports the available results of a numerical research effort currently under way and whose final goal is to assess and mechanically interpret the influence of the cross-section geometry and end support conditions on the elastic distortional post-buckling behavior and strength of cold-formed steel columns. This work deals only with simply supported (pinned end sections that can warp freely) columns exhibiting lipped channel, hat and zed cross-sections, which share common critical distortional buckling loads (for the same length and cross-section dimensions, of course) – *i.e.*, the columns eligible for this investigation are grouped into various column triplets. Initially, the paper presents the column geometry selection (cross-section dimensions and lengths), which involves sequences of “trial-and-error” buckling analyses based on Generalized Beam Theory (GBT) and leads to column triplets buckling in “pure” distortional modes and purposely exhibiting a wide range of cross-section proportions. Taking advantage of the GBT modal decomposition features, the buckling analyses are also used to mechanically characterize the various column critical buckling modes – in particular, their most relevant modal participations are identified and quantified, which may help in predicting the column post-buckling behavior and strength. Then, the paper presents and discusses results concerning the elastic post-critical strength of the selected column triplets, obtained from ANSYS shell finite element analyses – a representative sample of the corresponding equilibrium paths and post-buckling deformed configurations are also shown. In particular, the post-critical strength data are used to attempt identifying key parameters (*e.g.*, cross-section dimension ratios or critical buckling mode mechanical characteristics), in the sense that they play a pivotal role in influencing the features exhibited by the column distortional post-buckling behavior and strength. Finally, the paper closes with a few concluding remarks that also address the next steps of the current research effort.

1. Introduction

The structural efficiency of a given cold-formed steel member can only be adequately assessed after possessing in-depth information concerning its buckling and post-buckling behaviors, a task involving (i) the identification of the relevant buckling modes, (ii) the evaluation of the associated buckling stresses and (iii) the assessment of the corresponding post-buckling behavior/strength, which requires determining non-linear equilibrium paths, accounting for the presence of unavoidable initial imperfections and, possibly, also the influence of mode interaction phenomena. This information also plays a crucial role in the elaboration, validation and calibration of adequate design procedures for cold-

¹ Civil Engineering Program, COPPE, Federal University of Rio de Janeiro, Brazil. <alandes@coc.ufrj.br>

² Civil Eng. Dept., ICIST, Instituto Superior Técnico, Technical University of Lisbon, Portugal. <dcamotim@civil.ist.utl.pt>

³ Structural Engineering Department, São Carlos School of Engineering, University of São Paulo, Brazil. <cbasaglia@usp.br>

formed steel members. Indeed, it leads to the formulation of reliable and physically based models, which is the only way to reach rational and efficient (safe and accurate) member ultimate strength estimations.

In the particular case of members (columns or beams) exhibiting distortional critical buckling and failure modes, the most popular and widespread procedure to estimate their ultimate strength values is the use of the design curves/expressions prescribed by the Direct Strength Method (DSM – *e.g.*, Schafer 2008), which have already been included in the current North American (AISI 2007), Australian/New Zealand (AS/NZS 2005) and Brazilian (ABNT 2010) specifications for cold-formed steel structures. In the case of the columns, the DSM design curve was validated and calibrated against experimental and numerical ultimate strength data concerning exclusively (or, at least, “almost exclusively”) fixed-ended columns exhibiting a limited number of cross-section shapes and dimensions (mostly lipped channel, hat-section and rack-section columns). However, recent numerical investigations, namely those reported by Landesmann & Camotim (2011, 2013), Yap & Hancock (2011) and Dinis *et al.* (2012), identified several columns exhibiting ultimate strengths that are not adequately predicted by the current DSM design curve – in most cases the numerical values are overestimated). Such columns exhibited either (i) end support conditions other than fixed and warping-prevented, namely pinned or free end sections which can warp freely (Landesmann & Camotim 2011, 2013) or (ii) complex (stiffened) cross-section shapes that were not considered in the validation/calibration of the DSM design curve (Yap & Hancock 2011 and Dinis *et al.* 2012). The authors believe that the discrepancy between the numerical ultimate strengths and their DSM predictions has its roots on the variation of the column distortional post-critical strength with the cross-section geometry (shape and dimensions) and support conditions, and this belief set the goal for the research effort currently under way. The numerical results presented and discussed in this work, which constitute the very first step of the above research effort, concern exclusively simply supported (pinned end sections that can warp freely) with lipped channel, hat and zed cross-sections, which share common distortional buckling loads (for the same length and cross-section dimensions, of course). This means that such numerical results make it possible to assess how the cross-section dimensions and shape (within the limited triplet considered, which is quite particular) influence the column elastic distortional post-buckling behavior and post-critical strength.

1.1 Motivation, Objective and Scope of this Work

In the course of a numerical investigation on the DSM design, against distortional failures, of pin-ended and fixed-ended lipped channel and rack-section columns, the authors (Landesmann & Camotim 2010) literally “stumbled” on a rather unexpected finding: the current DSM design curve clearly overestimated the column ultimate strength *at room temperature* (this did not happen at all for the fixed-ended columns). This finding prompted an investigation on how the column end support condition influenced the quality of the DSM prediction of their distortional failure loads (Landesmann & Camotim 2011, 2013) – this involved (i) four end support conditions (fixed, fixed-pinned, pinned and fixed-free end sections), (ii) four cross-section shapes (lipped channels, hats, zeds and racks), (iii) a few (six or seven) mid-line dimensions per cross-section shape, selected to ensure pure buckling and failure modes⁴, and (iv) various yield stresses, selected in order to cover a wide distortional slenderness range. The chief conclusion of the above investigation consisted of the fact that, regardless of the cross-section shape, the current DSM distortional strength curve only predicts adequately (safely and accurately) the ultimate strength of fixed columns – all the remaining column ultimate strengths were found to be more or less overestimated, a surprising feature that was (rightly) attributed to the relevant stiffening role played by the end cross-section wall bending and (mostly) warping fixity. However, another behavioral feature emerged from the this study: the wide

⁴ The same cross-section dimensions were considered for the lipped channel, hat-section and zed-section columns.

variety of elastic post-buckling behaviors exhibited by the columns analyzed, even amongst those sharing the same cross-section shape and end support conditions – this led the authors to “pledge” that they would investigate this issue in the near future. The fulfillment of this “promise” provided the motivation for the research effort currently under way and whose first fruits are reported in this paper.

The objective of this paper is two-fold. First of all, to identify and mechanically characterize a significant number of simply supported (pinned end sections that can warp freely) columns exhibiting lipped channel, zed and hat cross-sections and buckling in “pure” distortional modes, in the sense that their critical distortional buckling loads are well below their local and global counterparts, thus precluding the occurrence of relevant mode interaction effects, *i.e.*, ensuring “truly distortional” post-buckling behaviors. Taking advantage of the fact that lipped channel, hat-section and zed-section columns share the same distortional (and local) buckling behavior, each set of cross-section dimensions and length identified defines a column triplet that is eligible for the present investigation. Then, the paper addresses the elastic (distortional) post-buckling behavior and strength of the various columns identified: a representative sample of the corresponding non-linear equilibrium paths are presented, analyzed, compared and, whenever possible, related to the buckling mode mechanical characteristics determined previously. The goal is to make an attempt to pin down key parameters (*e.g.*, cross-section dimension ratios or critical buckling mode mechanical characteristics), in the sense that they play a pivotal role in influencing the features exhibited by the column distortional post-buckling behavior and strength.

1.2 Outline of the Paper

The main body of the work carried out is presented in the next three sections of the paper. In order to make the issues addressed and their presentation easier to capture, the contents and objectives of each of these sections are briefly described and linked below:

- (i) Section 2 concerns the column geometry selection, achieved by means of time-consuming sequences of “trial-and-error” buckling analyses based on Generalized Beam Theory (GBT). The objective is to identify cross-section dimensions and lengths that lead to lipped channel, hat-section and zed-section columns exhibiting distortional buckling modes “as pure as possible” (and, if viable, fulfilling also a few additional requirements).
- (ii) Section 3 is devoted to the mechanical characterization of the critical (distortional) buckling modes of the column triplets identified in the previous item. This is done by means of GBT, taking advantage of its rather unique modal nature, and the objective is to obtain the most relevant deformation mode contributions to the various column critical distortional buckling modes⁵.
- (iii) After briefly describing the ANSYS shell finite element model adopted in this work, section 4 presents and discusses the elastic post-buckling behavior of the selected column triplets. Particular attention is paid to the comparative assessment of the various (iii₁) column non-linear equilibrium paths and (iii₂) post-critical strengths at a common deformation level (somewhat arbitrarily defined). Moreover, an attempt is made to correlate the significant variability of the column post-critical strength with geometrical and/or mechanical features, thus enabling a more or less reliable prediction.

2. Column Geometry Selection – Buckling Behavior

The first step consists of selecting the cross-section dimensions and lengths of the simply supported lipped channel (C), hat-section (H) and zed-section (Z) columns to be analyzed. At this stage, recall that

⁵ Only very rarely does a column “pure” distortional buckling mode exhibit a sole contribution from the GBT distortional deformation mode – usually, one or two local modes also participate in the column critical (distortional buckling) mode.

the end cross-sections of such columns exhibit (i) null in-plane local/global displacements and torsional rotations, and (ii) free local/global rotations and warping displacements. The selection procedure involved time-consuming sequences of “trial-and-error” buckling analyses, performed with the GBT-based code GBTUL (Bebiano *et al.* 2008a,b) and aimed at satisfying the following requirements:

- (i) Columns buckling in “pure” symmetric distortional modes. This goal is achieved by ensuring, as much as possible, that the critical buckling stress (i_1) is clearly distortional and (i_2) falls considerably below the lowest local and global bifurcation stresses.
- (ii) Cross-section dimensions not “too extreme” and involving wall proportions (*e.g.*, the web-to-flange width ratio b_w/b_f ratio) covering ranges as wide as possible. The fulfillment of this requirement will make it possible to assess whether such wall proportions play a meaningful role on the column distortional post-critical strength.
- (iii) Columns lengths (iii_1) corresponding to single half-wave buckling modes and (iii_2) as close as possible to the values associated with the minimum distortional critical buckling stress, as illustrated in Fig. 1 for the columns C-H-Z 60(6).

Fortunately, it was possible to fulfill all the above requirements and the end product of the “trial-and-error” selection procedure are the 44 column triplets (Cs, Hs and Zs) with identical cross-section dimensions and distortional buckling lengths L_D – they are given in Table 1, where it is worth noting that (i) the columns are ordered according to the web width b_w , (ii) several columns share the same b_w value and (iii) the b_w/b_f , b_w/t and b_f/b_l ratios range from 1.0 to 2.0, 27.3 to 61.1 and 3.8 to 15, respectively. On the other hand, Table 2 provides, for each selected column, the (i) critical (distortional) buckling load $P_{cr,D} \equiv P_{cr}$, (ii) ratios relating the critical local ($P_{cr,L}$), critical global ($P_{cr,G}$) and second (P_{b2}) bifurcation loads⁶ with P_{cr} , all obtained for $E=210\text{ GPa}$ (Young’s modulus) and $\nu=0.3$ (Poisson’s ratio) – in addition, the nature N and half-wave number hwn exhibited by the column second buckling modes are also given (between parenthesis – N_{hwn})⁷. The observation of these results prompts the following remarks:

- (i) As expected, the columns triplet exhibit virtually identical distortional and local bifurcation loads. Obviously, the global ones are clearly different (in value and/or nature): the $P_{cr,L}/P_{cr}$ and $P_{cr,G}/P_{cr}$ ratios range from 1.03-2.87 and 2.25-75.4, respectively. The lowest $P_{cr,L}/P_{cr}$ ratios concern the

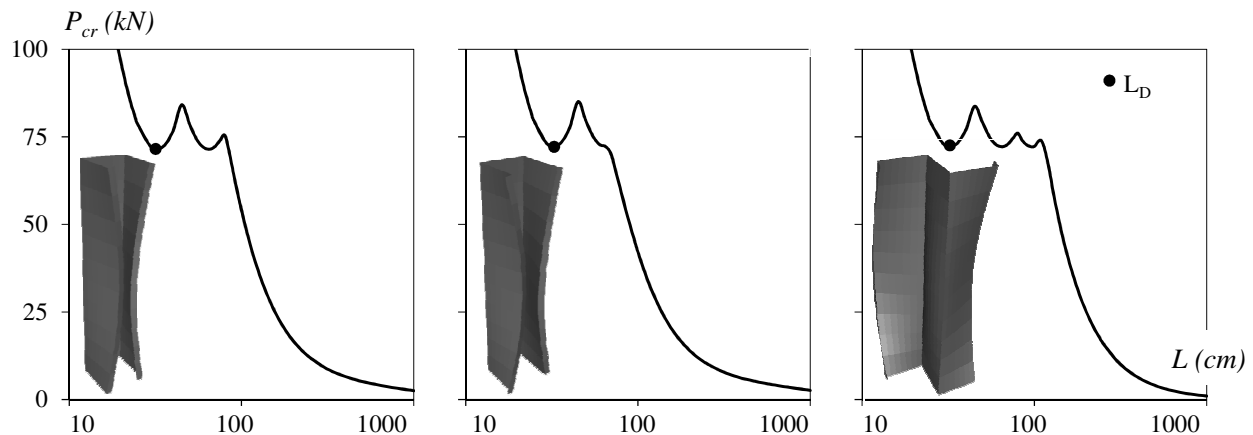


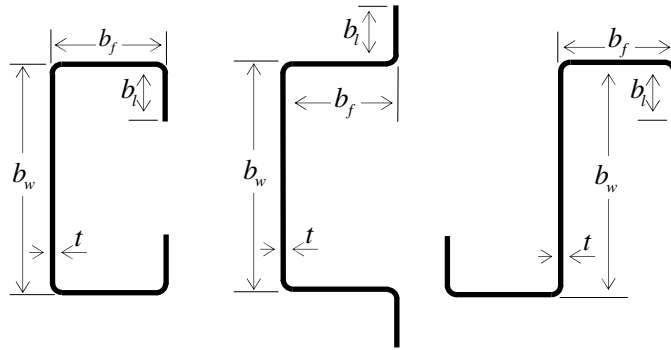
Figure 1: Curves P_{cr} vs. L concerning C-H-Z 60(6) columns with the indication of the selected lengths (L_D) and associated distortional buckling mode shapes.

⁶ They provide an indication concerning the “purity” of the column distortional post-buckling behaviour.

⁷ The nature of the second buckling mode may be symmetrical distortional (D), anti-symmetrical distortional (AD), local (L) or a combination of these –recall that the critical buckling mode is always D_1 (single half-wave symmetric distortional).

Table 1: Selected column cross-section dimensions and lengths

Column C-H-Z	b_w (mm)	b_f (mm)	b_l (mm)	t (mm)	L_D (cm)	Column C-H-Z	b_w (mm)	b_f (mm)	b_l (mm)	t (mm)	L_D (cm)
60(1)	60	60	5	1.5	30	110(2)	110	60	8	2.75	30
60(2)	60	60	5.75	1.5	30	110(3)	110	60	10	2.8	31
60(3)	60	60	6.5	1.5	30	110(4)	110	70	10	2.6	36
60(4)	60	60	7.25	1.5	30	110(5)	110	75	10	2.4	38
60(5)	60	60	8	1.4	30	110(6)	110	80	10	2.2	41
60(6)	60	60	8	1.5	30	110(7)	110	85	10	2	45
60(7)	60	60	8	1.6	30	110(8)	110	90	10	1.8	49
60(8)	60	60	8	1.8	30	116	116	72.5	9.7	2.9	34
60(9)	60	60	8	2	30	118	118	64.3	8.6	2.95	29
60(10)	60	60	8	2.2	30	120(1)	120	75	5	2	27
75	75	75	10	1.875	39	120(2)	120	75	5	3	24
80(1)	80	40	10	2.5	26	120(3)	120	75	5	4	22
80(2)	80	45	10	2.4	26	120(4)	120	75	10	2	42
80(3)	80	50	10	2	31	120(5)	120	75	10	3	35
80(4)	80	55	10	1.8	34	120(6)	120	75	10	4	30
80(5)	80	60	10	1.7	37	120(7)	120	75	20	3	57
80(6)	80	62	8	2	30	130	130	65	8.7	3.25	28
80(7)	80	65	10	1.6	40	140	140	100	10	3	43
80(8)	80	70	10	1.5	44	150	150	80	10	3	38
90	90	70	9.3	2.25	35	160	160	95	10	3	43
100	100	50	6.7	2.5	25	170	170	100	15	3.5	54
110(1)	110	55	10	3	28	180	180	95	15	4.2	48



C-H-Z120(7) and H80(1) columns, which are included in this investigation because (i₁) they buckle in a predominantly distortional mode and (i₂) exhibit peculiar behavioral features – their numerical post-buckling behavior will be specifically addressed ahead in the paper.

- (ii) For a clear majority (about 76%) of the selected H columns, the second buckling mode is single half-wave anti-symmetric distortional – in contrast, only about half of the C and Z columns exhibit a similar second buckling mode⁸.
- (iii) Moreover, regardless the second buckling mode nature, the P_{b2}/P_{cr} ratios concerning the C-Z column pairs are almost identical and vary between 1.09 and 1.51 – their H column counterparts are systematically lower and vary between 1.01 and 1.38.

⁸ A subset of their H column counterparts.

Table 2: Column distortional, local, global and second bifurcation loads and buckling mode

Column	Lipped channel				Hat-section				Zed-section			
	P_{cr} (kN)	$\frac{P_{cr.L}}{P_{cr}}$	$\frac{P_{cr.G}}{P_{cr}}$	$\frac{P_{b2}}{P_{cr}}(N_{nhw})$	P_{cr} (kN)	$\frac{P_{cr.L}}{P_{cr}}$	$\frac{P_{cr.G}}{P_{cr}}$	$\frac{P_{b2}}{P_{cr}}(N_{nhw})$	P_{cr} (kN)	$\frac{P_{cr.L}}{P_{cr}}$	$\frac{P_{cr.G}}{P_{cr}}$	$\frac{P_{b2}}{P_{cr}}(N_{nhw})$
60(1)	52.04	2.87	10.14	1.17(D ₂)	52.31	2.84	8.94	1.17(D ₂)	52.05	2.86	19.93	1.17(D ₂)
60(2)	55.48	2.66	9.75	1.35(D ₂)	55.85	2.64	8.30	1.23(AD ₁)	55.64	2.65	18.98	1.35(D ₂)
60(3)	59.89	2.46	9.27	1.4(AD ₁)	60.38	2.43	7.61	1.19(AD ₁)	60.20	2.44	17.86	1.42(AD ₁)
60(4)	65.29	2.25	8.74	1.38(AD ₁)	65.93	2.23	6.89	1.16(AD ₁)	65.73	2.23	16.64	1.39(AD ₁)
60(5)	62.14	1.93	8.81	1.36(AD ₁)	62.86	1.90	6.67	1.12(AD ₁)	62.63	1.91	16.59	1.35(AD ₁)
60(6)	71.68	2.06	8.19	1.37(AD ₁)	72.51	2.03	6.20	1.12(AD ₁)	72.25	2.04	15.40	1.36(AD ₁)
60(7)	82.26	2.18	7.62	1.37(AD ₁)	83.20	2.16	5.78	1.12(AD ₁)	82.91	2.16	14.31	1.38(AD ₁)
60(8)	106.78	2.41	6.62	1.39(AD ₁)	107.97	2.38	5.03	1.12(AD ₁)	107.53	2.39	12.41	1.41(AD ₁)
60(9)	136.24	2.60	5.78	1.39(AD ₁)	137.74	2.57	4.39	1.11(AD ₁)	136.95	2.58	10.81	1.43(AD ₁)
60(10)	171.16	2.77	5.07	1.38(AD ₁)	173.03	2.74	3.86	1.09(AD ₁)	171.61	2.75	9.48	1.44(D ₂)
75	111.32	2.08	7.63	1.38(AD ₁)	112.60	2.05	5.78	1.12(AD ₁)	112.22	2.06	14.32	1.39(AD ₁)
80(1)	362.16	1.25	4.88	1.20(L ₄)	407.25	1.11	3.00	1.09(L ₄)	365.33	1.24	5.14	1.19(L ₄)
80(2)	304.91	1.37	6.18	1.33(L ₄)	330.14	1.26	4.05	1.18(AD ₁)	307.19	1.36	7.31	1.31(L ₄)
80(3)	187.64	1.34	6.46	1.31(L ₅)	198.47	1.26	4.42	1.19(AD ₁)	189.23	1.33	8.43	1.3(L ₅)
80(4)	137.14	1.37	7.14	1.35(L ₅)	142.82	1.32	5.05	1.18(AD ₁)	138.27	1.36	10.15	1.34(L ₅)
80(5)	111.76	1.47	7.46	1.44(L ₅)	115.16	1.42	5.42	1.18(AD ₁)	112.68	1.45	11.43	1.42(L ₅)
80(6)	129.96	2.06	11.00	1.44(AD ₁)	132.45	2.01	8.86	1.23(AD ₁)	130.64	2.04	17.66	1.44(AD ₁)
80(7)	90.61	1.53	7.85	1.48(AD ₁)	92.68	1.49	5.83	1.17(AD ₁)	91.35	1.51	12.84	1.48(AD ₁)
80(8)	73.10	1.56	7.95	1.46(AD ₁)	74.38	1.54	6.00	1.17(AD ₁)	73.71	1.55	13.75	1.47(AD ₁)
90	168.15	2.02	10.12	1.45(AD ₁)	171.49	1.98	9.94	1.22(AD ₁)	169.09	2.01	16.25	1.45(AD ₁)
100	234.69	1.51	12.99	1.24(L+D ₂)	246.18	1.43	10.80	1.24(L+D ₂)	235.35	1.51	14.14	1.23(L+D ₂)
110(1)	408.01	1.37	10.27	1.29(L ₃)	439.90	1.27	7.60	1.22(L ₃)	409.10	1.37	11.15	1.28(L ₃)
110(2)	277.69	1.61	12.49	1.31(D+L ₂)	289.21	1.55	10.34	1.32(D+L ₂)	278.62	1.61	14.75	1.3(D+L ₂)
110(3)	328.03	1.45	10.66	1.37(L ₃)	347.23	1.36	8.12	1.32(L ₃)	329.26	1.44	12.55	1.36(L ₃)
110(4)	243.66	1.62	11.43	1.51(D+L ₂)	251.98	1.56	9.11	1.3(AD ₁)	244.77	1.61	15.52	1.49(D+L ₂)
110(5)	189.84	1.68	12.89	1.49(AD ₁)	194.93	1.63	10.44	1.28(AD ₁)	190.68	1.67	18.67	1.49(AD ₁)
110(6)	146.14	1.73	13.92	1.47(AD ₁)	149.25	1.69	11.42	1.27(AD ₁)	146.78	1.72	21.35	1.47(AD ₁)
110(7)	110.76	1.73	14.55	1.46(AD ₁)	112.66	1.70	12.07	1.27(AD ₁)	111.26	1.72	23.51	1.46(AD ₁)
110(8)	82.39	1.70	15.52	1.45(AD ₁)	83.55	1.68	13.00	1.27(AD ₁)	82.77	1.69	26.29	1.45(AD ₁)
116	295.58	1.76	13.28	1.5(AD ₁)	305.02	1.70	10.86	1.3(AD ₁)	296.67	1.76	17.81	1.5(D ₂)
118	314.76	1.61	15.54	1.41(L+D ₂)	327.93	1.53	12.86	1.37(AD ₁)	315.53	1.60	18.38	1.39(L+D ₂)
120(1)	76.12	2.13	34.90	1.41(AD ₁)	76.90	2.11	52.72	1.35(AD ₁)	76.18	2.13	75.41	1.41(AD ₁)
120(2)	217.57	2.62	36.87	1.36(AD ₁)	219.66	2.59	34.74	1.31(AD ₁)	217.71	2.62	49.52	1.36(AD ₁)
120(3)	470.67	2.87	26.75	1.32(AD ₁)	474.93	2.82	25.22	1.27(AD ₁)	470.60	2.87	35.84	1.32(AD ₁)
120(4)	123.96	1.31	15.90	1.28(L ₄)	128.01	1.27	12.98	1.24(L ₄)	124.35	1.31	21.41	1.27(L ₄)
120(5)	315.54	1.77	13.43	1.5(AD ₁)	325.56	1.71	10.99	1.3(AD ₁)	316.69	1.76	18.01	1.5(AD ₁)
120(6)	626.45	2.08	12.19	1.44(AD ₁)	645.74	2.01	9.99	1.26(AD ₁)	628.51	2.08	16.29	1.44(AD ₁)
120(7)	517.35	1.12	4.00	1.11(L ₆)	561.12	1.03	2.25	1.01(AD ₁)	525.13	1.10	4.99	1.09(L ₆)
130	386.75	1.54	17.81	1.34(L ₂)	405.70	1.46	14.81	1.33(L ₂)	387.28	1.55	19.47	1.33(L ₂)
140	234.97	2.12	20.72	1.43(AD ₁)	236.79	2.08	18.12	1.3(AD ₁)	233.89	2.11	31.52	1.43(AD ₁)
150	286.24	1.44	20.00	1.35(L ₃)	295.26	1.38	16.88	1.32(L ₃)	284.62	1.44	23.25	1.34(L+D ₂)
160	244.33	1.66	24.52	1.45(D+AD ₂)	248.55	1.62	21.48	1.38(AD ₁)	243.10	1.66	31.55	1.44(D+L ₂)
170	442.24	1.36	12.82	1.32(L ₄)	458.51	1.30	10.11	1.28(L ₄)	441.13	1.36	16.26	1.32(L ₄)
180	690.56	1.38	13.06	1.30(L ₃)	725.78	1.30	10.20	1.25(L ₃)	688.30	1.38	14.98	1.3(L ₃)

3. Buckling Mode Mechanical Characterization

This section addresses the mechanical characterization of the critical buckling modes of the selected column triplets – the objective is to assess and quantify the natures of the deformations involved in the various column critical distortional buckling modes⁹. This is straightforwardly done by means of GBT, taking advantage of (i) its rather unique modal features and (ii) the fact that the selected column geometries were obtained from buckling analyses carried out in the code GBTUL, which automatically provides the GBT modal decomposition of the column buckling modes¹⁰. Figure 2 displays the in-plane configurations of the C-H-Z 110(5) column GBT deformation modes that are most relevant for the present investigation, namely the (i) symmetric (5) and anti-symmetric (6) distortional modes, and (ii) two local (7 and 9) modes – all the remaining columns exhibit qualitatively similar deformation modes¹¹. Table 3 provides the contributions of the GBT deformation modes to the critical buckling modes of all the column triplets considered in this study – p_n stands for the percentage participation of GBT deformation mode n (this modal decomposition is illustrated in Fig. 3, showing the buckled mid-span cross-section of the C 110(5) column). From the observation of these results, the following conclusions can be drawn:

- (i) All critical buckling modes combine a highly dominant participation from symmetric distortion (p_5) with minor (but non negligible) contributions from web-triggered local deformations (p_7 and p_9).

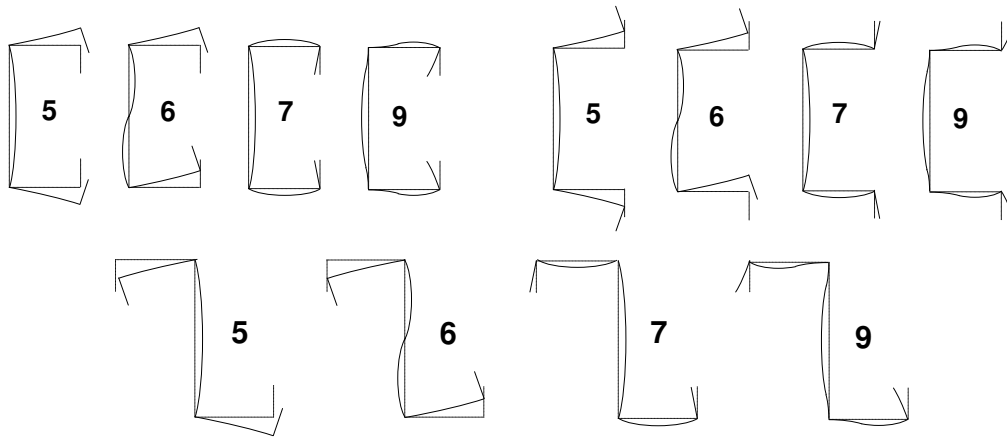


Figure 2: Configurations of the C-H-Z 110(5) column GBT deformation modes (i) 5 (symmetric distortional), (ii) 6 (anti-symmetric distortional) and (iii) 7 + 9 (web-triggered local)

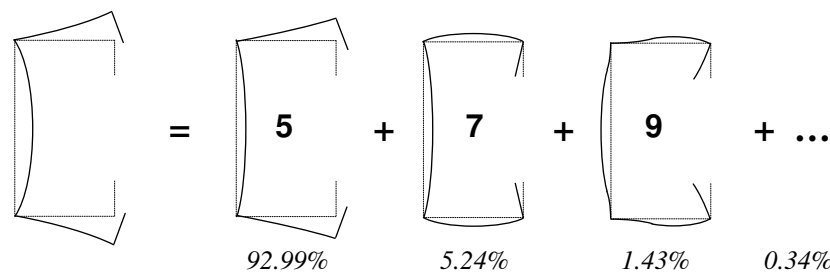


Figure 3: Illustrative GBT modal decomposition: distortional buckled mid-span cross-section of the C 110(5) column

⁹ The so-called column “pure” distortional buckling modes invariably exhibit a more or less significant amount of local deformations, exclusively associated with transverse wall bending.

¹⁰ In order to acquire information about the basic concepts of procedures involved in the performance of a GBT buckling analysis, the interested reader should visit the works of Silvestre & Camotim (2002a,b), Camotim et al. (2004) and Dinis *et al.* (2006).

¹¹ In the light of these modal features of the GBT buckling analyses, it becomes clear how the natures of the column second buckling modes, given in Table 2, were determined.

Table 3: GBT modal decomposition of the selected column critical buckling modes

Column	Lipped channel					Hat-section					Zed-section				
	p_5	p_7	p_9	p_{7+9}	p_{others}	p_5	p_7	p_9	p_{7+9}	p_{others}	p_5	p_7	p_9	p_{7+9}	p_{others}
60(1)	93.9	4.2	1.5	5.7	0.4	94.0	4.2	1.6	5.8	0.2	91.1	4.2	1.5	5.7	3.2
60(2)	94.0	4.2	1.4	5.6	0.4	94.1	4.1	1.5	5.6	0.3	91.4	4.2	1.4	5.6	3.0
60(3)	94.0	4.2	1.4	5.6	0.4	94.1	4.1	1.5	5.6	0.3	91.5	4.2	1.4	5.6	2.9
60(4)	94.0	4.3	1.3	5.6	0.4	94.1	4.2	1.4	5.6	0.3	91.5	4.3	1.3	5.6	2.9
60(5)	93.4	4.8	1.4	6.2	0.4	93.6	4.6	1.5	6.1	0.3	91.1	4.8	1.4	6.2	2.7
60(6)	93.8	4.4	1.3	5.7	0.5	94.0	4.3	1.4	5.7	0.3	91.3	4.5	1.3	5.8	2.9
60(7)	94.1	4.2	1.3	5.5	0.4	94.2	4.2	1.4	5.6	0.2	91.5	4.2	1.3	5.5	3.0
60(8)	94.6	3.7	1.2	4.9	0.5	94.7	3.7	1.3	5.0	0.3	91.4	3.9	1.2	5.1	3.5
60(9)	95.0	3.4	1.1	4.5	0.5	95.1	3.4	1.2	4.6	0.3	91.3	3.5	1.1	4.6	4.1
60(10)	95.3	3.2	1.1	4.3	0.4	95.4	3.2	1.2	4.4	0.2	91.1	3.3	1.1	4.4	4.5
75	95.3	3.3	1.0	4.3	0.4	95.5	3.2	1.1	4.3	0.2	93.2	3.4	1.0	4.4	2.4
80(1)	87.3	8.7	0.9	9.6	3.1	91.1	6.9	1.1	8.0	0.9	87.6	9.2	0.9	10.1	2.3
80(2)	89.4	7.6	1.2	8.8	1.8	91.9	6.1	1.4	7.5	0.6	89.6	8.0	1.2	9.2	1.2
80(3)	91.7	5.9	1.2	7.1	1.2	93.4	4.9	1.3	6.2	0.4	90.8	6.1	1.2	7.3	1.9
80(4)	92.7	5.2	1.2	6.4	0.9	94.0	4.5	1.3	5.8	0.2	91.4	5.3	1.2	6.5	2.1
80(5)	93.7	4.5	1.1	5.6	0.7	94.5	4.1	1.2	5.3	0.2	92.0	4.6	1.1	5.7	2.3
80(6)	92.7	5.2	1.5	6.7	0.6	93.1	4.9	1.6	6.5	0.4	91.3	5.3	1.6	6.9	1.8
80(7)	94.4	4.1	1.0	5.1	0.5	94.9	3.8	1.1	4.9	0.2	92.6	4.2	1.0	5.2	2.2
80(8)	94.9	3.6	0.9	4.5	0.6	95.3	3.4	1.1	4.5	0.2	93.1	3.7	1.0	4.7	2.2
90	93.8	4.5	1.3	5.8	0.4	94.2	4.1	1.4	5.5	0.3	92.4	4.5	1.3	5.8	1.8
100	86.0	11.2	1.5	12.7	1.3	87.0	10.5	1.6	12.1	0.9	86.4	11.5	1.5	13.0	0.6
110(1)	87.0	10.4	1.2	11.6	1.4	88.6	9.2	1.4	10.6	0.8	87.1	10.8	1.2	12.0	0.9
110(2)	89.7	7.9	1.4	9.3	1.0	90.5	7.2	1.5	8.7	0.8	89.7	8.1	1.4	9.5	0.8
110(3)	89.6	8.1	1.3	9.4	1.0	90.8	7.1	1.4	8.5	0.7	89.6	8.4	1.3	9.7	0.7
110(4)	92.5	5.5	1.4	6.9	0.6	93.2	4.9	1.5	6.4	0.4	91.9	5.6	1.4	7.0	1.1
110(5)	92.9	5.2	1.4	6.6	0.5	93.5	4.7	1.5	6.2	0.3	92.2	5.3	1.4	6.7	1.1
110(6)	93.4	4.8	1.3	6.1	0.5	93.8	4.5	1.4	5.9	0.3	92.6	4.9	1.3	6.2	1.2
110(7)	94.0	4.4	1.2	5.6	0.4	94.3	4.2	1.3	5.5	0.2	93.2	4.5	1.2	5.7	1.1
110(8)	94.4	4.2	1.1	5.3	0.3	94.6	4.0	1.1	5.1	0.3	93.6	4.2	1.1	5.3	1.1
116	92.0	5.9	1.5	7.4	0.6	92.7	5.3	1.6	6.9	0.4	91.5	6.0	1.5	7.5	1.0
118	88.8	8.9	1.6	10.5	0.7	89.6	8.1	1.7	9.8	0.6	88.8	9.0	1.6	10.6	0.6
120(1)	87.7	8.8	3.0	11.8	0.5	88.0	8.5	3.0	11.5	0.5	87.5	8.8	3.0	11.8	0.7
120(2)	91.2	5.3	2.8	8.1	0.7	91.5	5.0	2.9	7.9	0.6	90.9	5.3	2.9	8.2	0.9
120(3)	93.6	2.8	2.7	5.5	0.9	93.9	2.5	2.8	5.3	0.8	93.2	2.7	2.8	5.5	1.3
120(4)	91.7	6.4	1.4	7.8	0.5	92.3	5.9	1.5	7.4	0.3	91.3	6.6	1.4	8.0	0.7
120(5)	92.2	5.7	1.5	7.2	0.6	92.9	5.2	1.6	6.8	0.3	91.7	5.8	1.5	7.3	1.0
120(6)	92.5	5.3	1.6	6.9	0.6	93.1	4.7	1.7	6.4	0.5	91.9	5.4	1.6	7.0	1.1
120(7)	95.2	3.0	0.5	3.5	1.3	96.9	2.1	0.6	2.7	0.4	94.8	3.1	0.5	3.6	1.6
130	86.3	11.4	1.5	12.9	0.8	87.1	10.6	1.6	12.2	0.7	86.4	11.6	1.5	13.1	0.5
140	93.7	4.5	1.5	6.0	0.3	93.9	4.2	1.5	5.7	0.4	93.2	4.5	1.5	6.0	0.8
150	89.4	8.7	1.3	10.0	0.6	90.1	8.0	1.4	9.4	0.5	89.4	8.8	1.3	10.1	0.5
160	91.7	6.4	1.4	7.8	0.5	92.1	6.0	1.5	7.5	0.4	91.5	6.5	1.5	8.0	0.5
170	93.7	4.9	0.9	5.8	0.5	94.3	4.3	1.0	5.3	0.4	93.5	5.0	0.9	5.9	0.6
180	92.0	6.4	0.9	7.3	0.7	92.8	5.7	1.0	6.7	0.5	92.1	6.6	0.9	7.5	0.4

While the former varies in the ranges 86.0-95.4 (Cs), 87.0-97.0 (Hs) and 86.4-93.6 (Zs), the joint contribution of the latter (p_{7+9}) amounts to 3.5-12.9 (Cs), 4.3-12.2 (Hs) and 3.6-13.1 (Zs). The participation of the other deformation modes never exceeds 4.5% and is below 1.0% in most cases.

- (ii) Figure 4, which plots p_5, p_7 and p_9 against the b_w/b_f ratio for all column triplets considered, shows that there are clear (and opposite) trends concerning the variation of both p_5 and p_7 with b_w/b_f . Indeed, it is observed that p_5 (p_7) decreases (increases) as b_w/b_f grows a bit more than linearly (almost parabolic variation) for every cross-section shape, which probably stems from the higher vulnerability of wider webs to local deformations. Conversely, no tendency is detected in any of the three p_9 vs. b_w/b_f plots.
- (iii) Figure 5, which plots p_5 against the b_w/t and b_f/b_l ratios for the column triplets examined, provides evidence that there is little correlation between these three quantities.

In the next section, the above findings will be used in the search for whether any correlation can be established between the critical buckling mode GBT modal decomposition and the column post-buckling behavior and/or post-critical strength. At the outset, it seems logical to anticipate that the presence of larger local deformations in the critical buckling mode will entail higher stiffness and strength levels.

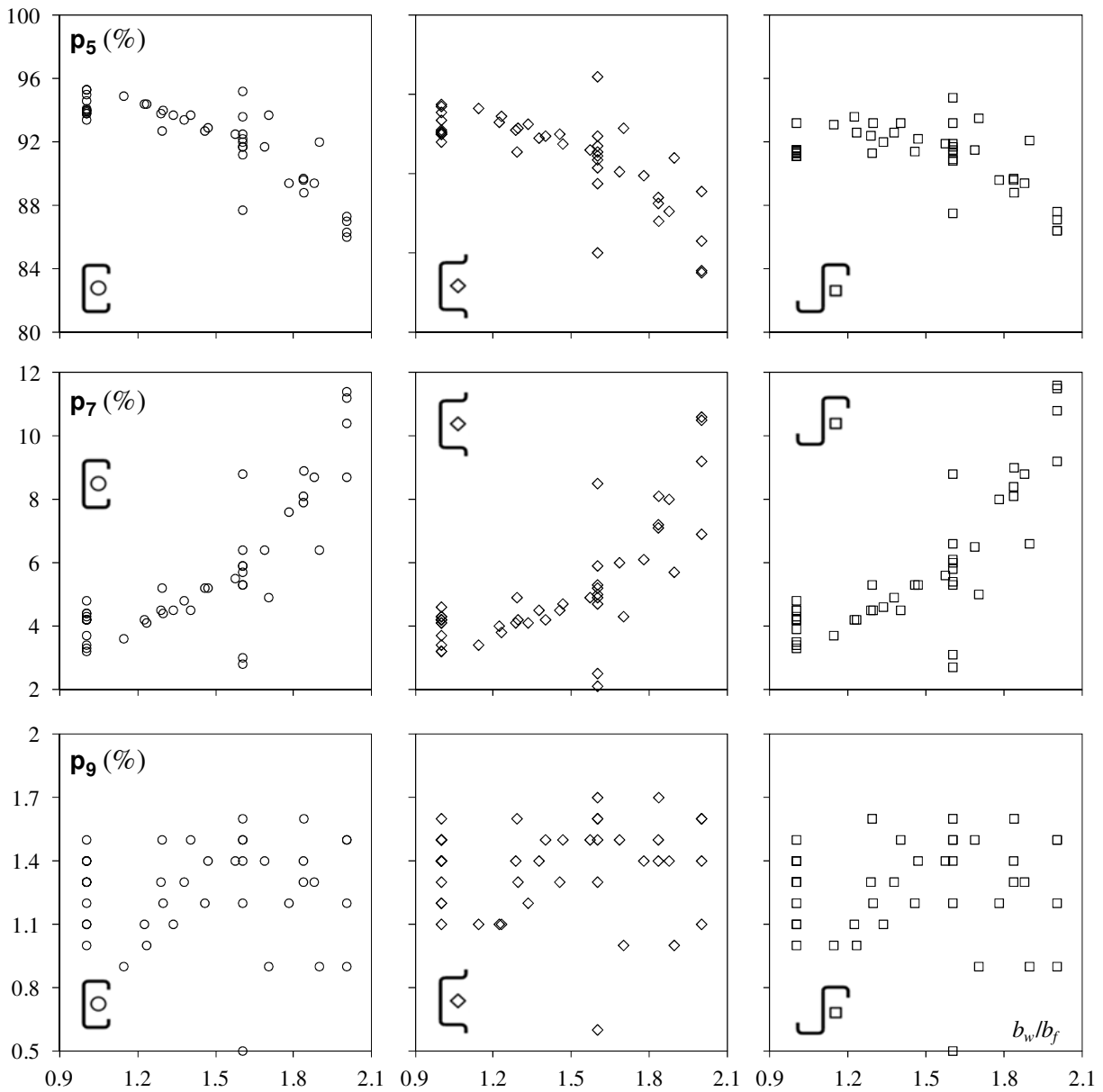


Figure 4: Variation of p_5, p_7 and p_9 with b_w/b_f

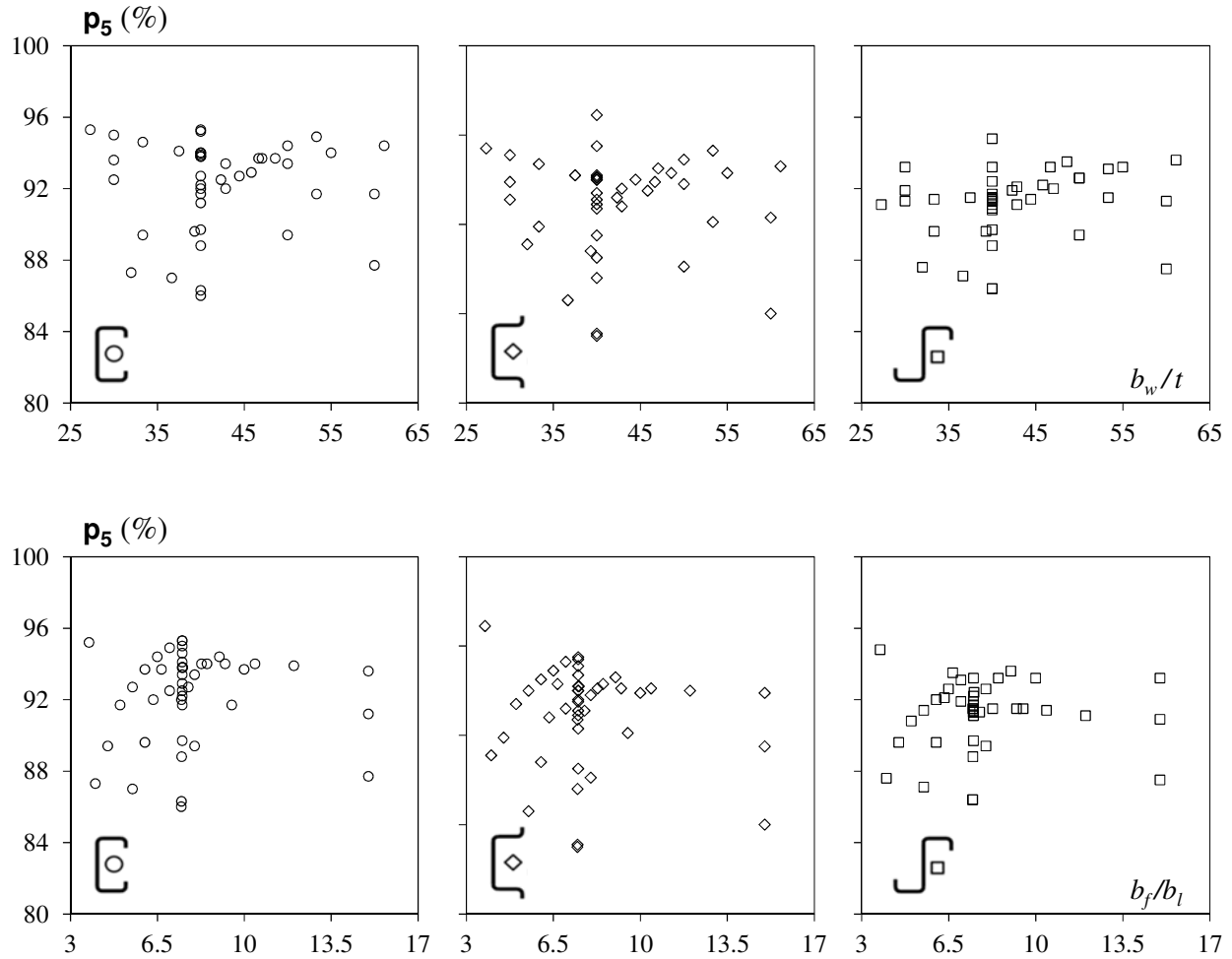


Figure 5: Variation of p_5 with b_w/t and b_f/b_l

4. Elastic Post-Buckling Behavior and Strength

After providing a brief description of the numerical model adopted to perform the geometrically non-linear ANSYS shell finite element analyses, the results concerning the elastic distortional post-buckling behavior and strength of the column triplets selected in section 2 are presented and discussed in detail.

4.1 Numerical Model

The column distortional post-buckling equilibrium paths were determined through geometrically non-linear SFEA carried out in the code ANSYS (SAS 2009). The columns were discretized into SHELL181 elements (4-node shear deformable thin-shell elements with six degrees of freedom per node and full integration) – previous convergence studies showed that $5\text{ mm} \times 5\text{ mm}$ meshes provide quite accurate results, even if at the cost of a fairly high computational effort. The analyses were performed by means of an incremental-iterative technique combining Newton-Raphson’s method with an arc-length control strategy. All columns exhibited (i) a linear elastic material behavior ($E=210\text{ GPa}$ and $\nu=0.3$) and (ii) critical-mode (distortional) initial geometrical imperfections with small amplitudes (10% of the wall thickness t). Their incorporation in the columns was made automatically by means of the following procedure (e.g., Dinis & Camotim 2013): (i) determination of the critical buckling mode shape, through an ANSYS SFE buckling analysis adopting exactly the same discretization/mesh employed to carry out the

subsequent post-buckling analysis, which was then (ii) scaled to exhibit maximum vertical displacements along the flange-stiffener longitudinal edges equal to $0.1t$ – this buckling analysis output is then “transformed” into an input of the non-linear analysis. Following the column distortional post-buckling asymmetry first unveiled by Prola & Camotim (2002a,b) and later also studied by Silvestre & Camotim (2006), these initial imperfections involve outward (Cs) and inward (Hs) flange-stiffener motions (those shown to lead to the lower post-buckling strengths) – obviously, this distinction makes no sense in the Z columns, since their flange-stiffener motions are always opposite (one outward and the other inward).

Concerning the modeling of the end support conditions, the membrane and bending transverse displacements were prevented at all end section nodes, while keeping the axial (warping) displacements and all the bending rotations free. To enable the load application, the rigid-body axial translation is free at both end sections – the axial compression is applied by means of a set of point loads acting on both end section nodes and increased in small increments, through the ANSYS automatic load stepping procedure.

4.2 Results and Discussion

These results presented and discussed consist of elastic post-buckling equilibrium paths that are then used to make a comparative assessment of the post-critical strength exhibited by the various columns. In order to illustrate the results obtained and also address the qualitative and quantitative assessment of how the column elastic distortional post-critical strength is influenced by the cross-section shape and dimensions, Fig. 6 depicts the equilibrium paths of the C-H-Z 60(6) and C-H-Z 100 columns, plotting the applied load P , normalized w.r.t. P_{cr} , against $|\delta|/t$, where $|\delta|$ is the absolute value of the mid-span (maximum) flange-stiffener corner vertical displacement¹² and t is the wall thickness. In order to achieve a more rational and meaningful comparison between the various equilibrium paths and post-critical strengths, it was decided to focus on strength values associated with $|\delta|/t=10$, hereafter designated as P_{10t} and corresponding to the black dots drawn on the P/P_{cr} vs. $|\delta|/t$ curves in Fig. 6. Finally, Fig. 7(a) depicts the C-H-Z 60(6)/100 column deformed configurations occurring for P_{10t} on each equilibrium path displayed in Fig. 6.

As noted earlier, following the performance of the buckling analyses, (i) the C-H-Z 120(7) and H 80(1) columns exhibited considerably low $P_{cr,1}/P_{cr}$ ratios ($1.12-1.03-1.10$ and 1.11 , respectively), and, in addition, (ii) column H 120(7) also exhibits almost coincident P_{b2} and P_{cr} loads (1.01 ratio), the latter being associated with anti-symmetric distortion (mode **6**). In view of these facts, these columns

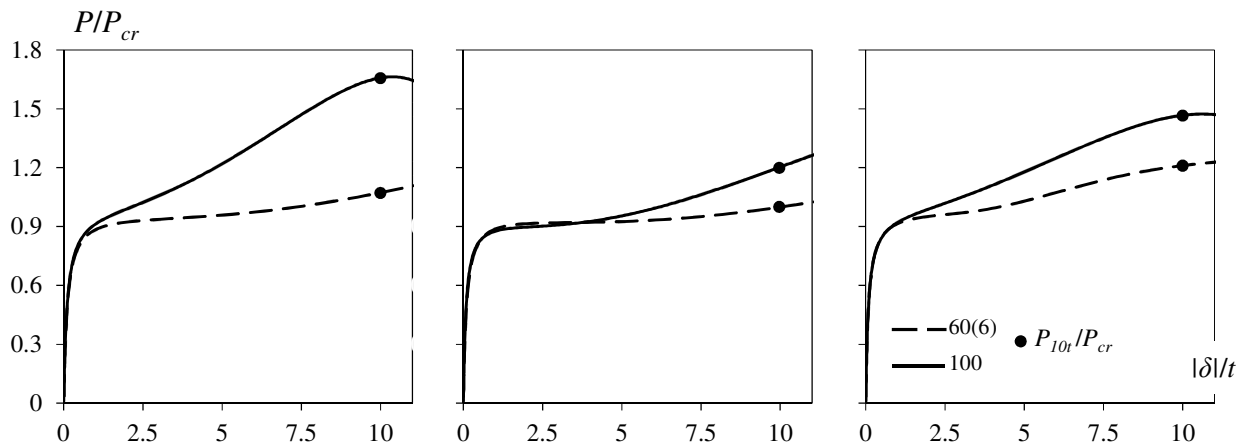


Figure 6: Elastic post-buckling equilibrium paths P/P_{cr} vs. $|\delta|/t$ concerning the C-H-Z 60(6)/100 columns

¹²In the Z-section columns, $|\delta|$ always concern the flange-stiffener moving inwards.

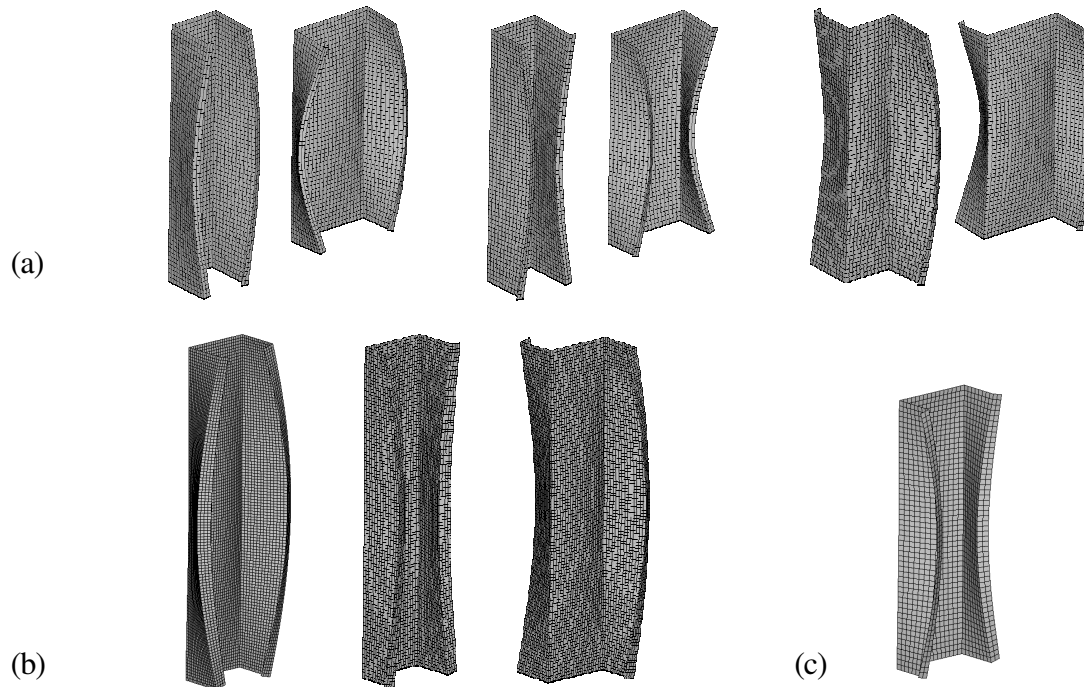


Figure 7: Post-buckling deformed configurations at $P=P_{10t}$ concerning the (a) C-H-Z 60(6)/100, (b) C-H-Z 120(7) and (c) H 80(1) columns

were expected to experience local/distortional and distortional/distortional (5-6) interaction, respectively. However, the subsequent inspection of their numerical post-buckling equilibrium paths and deformed configurations modes did not confirm these predictions, as no traces of interaction were detected¹³ – the post-buckling ($P=P_{10t}$) deformed configurations of the C-H-Z-120(7) and H-80(1) columns are shown in Figs. 7(b) and 7(c), respectively. Instead, these post-buckling deformed configurations involve only symmetric distortional deformations (similar to the C-H-Z 60(6)/100 column ones and akin to the critical buckling mode and deformation mode 5) and, thus, these columns were kept in this investigation.

Table 4 shows, for each column triplet included in Table 1, (i) the cross-section proportions, defined by the b_w/b_f , b_w/t and b_f/b_l ratios, and (ii) the elastic post-critical strength P_{10t} . In order to assess the variation of P_{10t} with the columns cross-section shape and dimension concerning, Fig. 8 plots P_{10t}/P_{cr} against b_w/b_f , b_w/t and b_f/b_l – nine plots, one for each combination of width ratio and cross-sections shape (note that the abscissa values and scales are not the same). The close observation of the results presented in Table 4 and Figs. 6 to 8 prompts the following remarks:

- (i) First of all, it is worth recalling the quite visible differences between the elastic equilibrium paths P/P_{cr} vs. $|\delta|/t$ displayed Fig. 6: the 100 columns ($b_w/b_f=2$) exhibit considerably higher post-critical strengths than their 60(6) counterparts ($b_w/b_f=1$). Moreover, note that the lipped channel and zed-section columns exhibit a limit point just after $|\delta|=10t$ ¹⁴, which implies that the “ductility” prior to failure also varies considerably with the column cross-section shape and dimensions.

¹³The post-buckling deformed configurations of all the columns with $P_{cr,L}/P_{cr}$ and P_{b2}/P_{cr} close to 1.0 (indeed, the criterion <2.0 was adopted) were carefully inspected to look for evidence of interaction. Nevertheless, it should be mentioned that only critical-mode initial geometrical imperfections included in the analyses – the above assertion may not remain valid if initial geometrical imperfections with other configurations are considered.

¹⁴During the selection procedure, involving a combination of “trial-and-error” buckling and post-buckling analyses, the columns exhibiting a *limit point* prior to reaching $|\delta|=10t$ were excluded from the present investigation.

Table 4: Column cross-section proportions (width ratios) and elastic post-critical strengths (P_{10t})

Column (C-H-Z)	b_w/b_f	b_w/t	b_f/b_l	P_{10t}/P_{cr}			Column (C-H-Z)	b_w/b_f	b_w/t	b_f/b_l	P_{10t}/P_{cr}		
				C	H	Z					C	H	Z
60(1)	1.00	40.00	12.00	1.20	1.11	1.11	110(2)	1.83	40.00	7.50	1.53	1.14	1.43
60(2)	1.00	40.00	10.43	1.17	1.08	1.10	110(3)	1.83	39.29	6.00	1.46	1.06	1.36
60(3)	1.00	40.00	9.23	1.13	1.05	1.08	110(4)	1.57	42.31	7.00	1.29	1.03	1.34
60(4)	1.00	40.00	8.28	1.10	1.02	1.06	110(5)	1.47	45.83	7.50	1.23	1.03	1.33
60(5)	1.00	42.86	7.50	1.05	0.99	1.03	110(6)	1.38	50.00	8.00	1.17	1.01	1.29
60(6)	1.00	40.00	7.50	1.06	1.00	1.04	110(7)	1.29	55.00	8.50	1.11	1.00	1.26
60(7)	1.00	37.50	7.50	1.09	1.01	1.04	110(8)	1.22	61.11	9.00	1.07	0.98	1.42
60(8)	1.00	33.33	7.50	1.12	1.03	1.05	116	1.60	40.00	7.47	1.38	1.11	1.40
60(9)	1.00	30.00	7.50	1.14	1.04	1.04	118	1.84	40.00	7.48	1.59	1.22	1.49
60(10)	1.00	27.27	7.50	1.16	1.04	1.02	120(1)	1.60	60.00	15.00	1.63	1.45	1.70
75	1.00	40.00	7.50	1.05	0.99	1.23	120(2)	1.60	40.00	15.00	1.81	1.58	1.75
80(1)	2.00	32.00	4.00	1.43	0.88	1.13	120(3)	1.60	30.00	15.00	1.77	1.63	1.74
80(2)	1.78	33.33	4.50	1.36	0.94	1.20	120(4)	1.60	60.00	7.50	1.18	0.99	1.29
80(3)	1.60	40.00	5.00	1.20	0.92	1.13	120(5)	1.60	40.00	7.50	1.39	1.11	1.40
80(4)	1.45	44.44	5.50	1.12	0.93	1.08	120(6)	1.60	30.00	7.50	1.48	1.24	1.38
80(5)	1.33	47.06	6.00	1.07	0.93	1.05	120(7)	1.60	40.00	3.75	1.12	0.86	1.08
80(6)	1.29	40.00	7.75	1.21	1.05	1.32	130	2.00	40.00	7.47	1.74	1.33	1.56
80(7)	1.23	50.00	6.50	1.04	0.94	1.03	140	1.40	46.67	10.00	1.34	1.15	1.45
80(8)	1.14	53.33	7.00	1.02	0.94	1.01	150	1.88	50.00	8.00	1.54	1.18	1.52
90	1.29	40.00	7.53	1.18	1.03	1.30	160	1.68	53.33	9.50	1.43	1.18	1.51
100	2.00	40.00	7.46	1.65	1.20	1.47	170	1.70	48.57	6.67	1.28	1.00	1.34
110(1)	2.00	36.67	5.50	1.59	1.10	1.36	180	1.89	42.86	6.33	1.50	1.09	1.42

- (ii) Regardless the cross-section dimensions, the lipped channel and zed-section columns exhibit higher post-critical strengths than their hat-section counterparts (this difference is clearly visible in Fig. 6).
- (iii) Figure 8 shows that there is substantial scatter in the plots showing the variation of P_{10t}/P_{cr} with b_w/b_f , b_w/t and b_f/b_l . Indeed, these values vary between (iii₁) 1.02 and 1.81 (Cs – average and standard deviation equal to 1.30 and 0.22), (iii₂) 0.86 and 1.63 (Hs – average and standard deviation equal to 1.08 and 0.16), and (iii₃) 1.01 and 1.75 (Zs – average and standard deviation equal to 1.28 and 0.21) – these values confirm the assertion made in the previous item.
- (iv) The comparison between the three sets of plots in Fig. 8 provides clear evidence that, unlike their b_w/t and b_f/b_l counterparts, the b_w/b_f ratios show some correlation with the normalized column post-critical strengths P_{10t}/P_{cr} . In fact, it is observed that P_{10t}/P_{cr} generally increases with b_w/b_f , a feature that is more perceptible for the lipped channel columns and less so for the hat-section and zed-section columns. Moreover, note also that the lipped channel column P_{10t}/P_{cr} values exhibit a much narrower dispersion than those concerning the hat-section and (mostly) zed-section columns – in the lipped channel and hat-section columns, this dispersion appears to grow slightly with b_w/b_f .
- (v) Since the C-Z-H 60(1-10) and 120(1-7) columns share the same web-to-flange width ratio (b_w/b_f equal to 1.0 and 1.60, respectively), their P_{10t}/P_{cr} values are located on the same vertical line in the P_{10t}/P_{cr} vs. b_w/b_f plots. The vertical dispersions exhibited by these values provide an indication of the combined influence of the b_w/t and b_f/b_l ratios, which vary within each column set. Because these vertical dispersions are much higher for $b_w/b_f=1.6$ than for $b_w/b_f=1.0$, it seems fair to conclude that the combined influence of b_w/t and b_f/b_l on P_{10t}/P_{cr} increases with b_w/b_f .

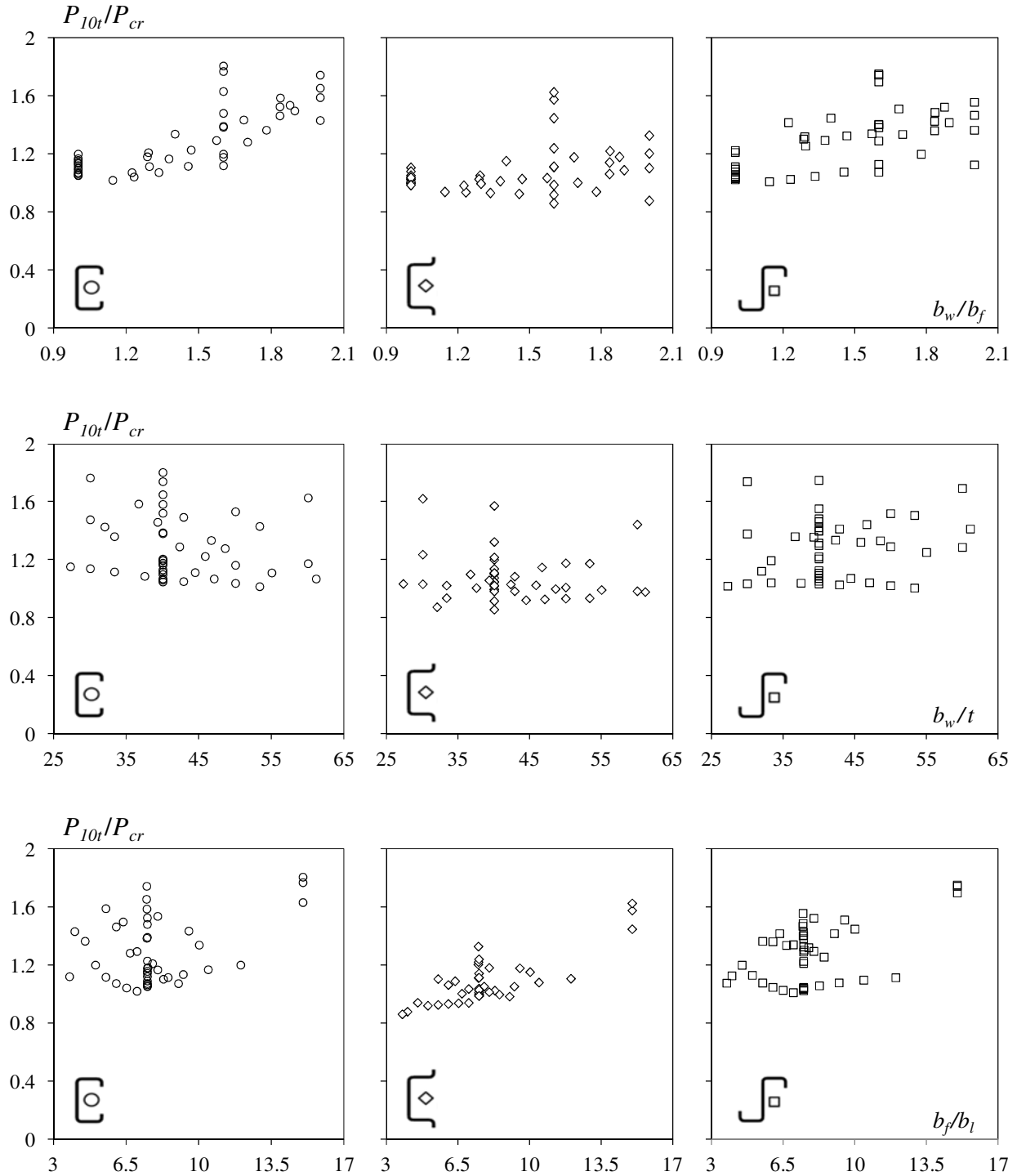


Figure 8: Variation of P_{10t}/P_{cr} with b_w/b_f , b_w/t and b_f/b_l

In an attempt to capture the influence of each individual width ratio on the column elastic distortional post-critical strength, Fig. 9 depicts the variations of P_{10t}/P_{cr} with each of the b_w/b_f , b_w/t and b_f/b_l width ratios, while keeping the remaining two constant (their values are also given in Fig. 9) – again nine plots, one per combination of variable width ratio¹⁵. The analysis of this limited amount of results suggests that:

¹⁵Of course, it was not an easy task to find sequence of column cross-section dimensions differing only in one width ratio.

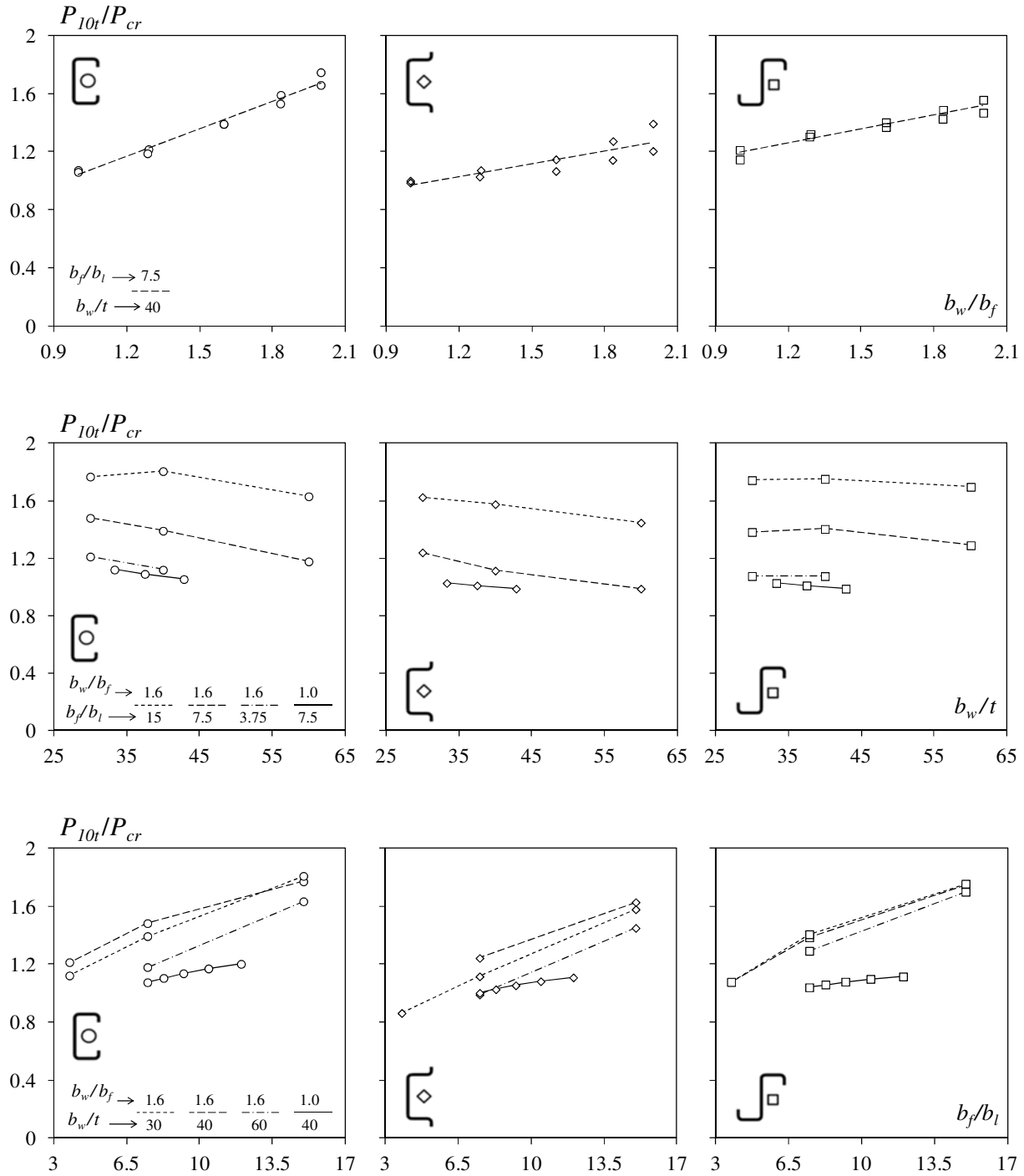


Figure 9: Variation of P_{10t}/P_{cr} with each individual width ratio b_w/b_f , b_w/t and b_f/b_l (the remaining two are kept constant)

- (i) By far the best documented P_{10t}/P_{cr} variations are those associated with the b_w/b_f ratio, which involve the C-H-Z 60(6)/75/80(6)/90/100/110(2)/116/118/120(7)/130 columns – b_w/b_f varies between 1.0 and 2.0, while $b_w/t=40$ and $b_f/b_l=7.50$ are kept constant. The variations of P_{10t}/P_{cr} with b_w/b_f follow roughly ascending straight lines with slopes that are cross-section dependent – the highest concerns the lipped channel columns and those corresponding to the hat-section and zed-section columns are fairly identical (the former is almost twice the latter).

- (ii) Although the variation of P_{10t}/P_{cr} with the b_w/t is poorly documented (no more than three columns sharing the same b_w/b_f and b_f/b_l combination), it seems possible to conclude that a b_w/t increase tends to slightly lower the column post-critical strength – the P_{10t}/P_{cr} drop is smaller for the zed-section columns. Moreover, the amount of the drop appears not to depend significantly on either the cross-section shape or the b_w/b_f and b_f/b_l combination – indeed the various straight line segments appearing in the three plots are “almost parallel”.
- (iii) Lastly, the variation of P_{10t}/P_{cr} with b_f/b_l falls somewhere in between the previous two, as far as the quality of the documentation is concerned (there are five columns sharing the same b_w/b_f and b_w/t combination). Regardless of the cross-section shape, the P_{10t}/P_{cr} value increases steeply with b_f/b_l . The slope of the P_{10t}/P_{cr} vs. b_f/b_l plot is almost independent of either the cross-section shape or the b_w/t ratio – however, it seems to decrease with b_f/b_l (even if only two values are considered).

Finally, Fig. 10 plots the P_{10t}/P_{cr} values against p_5 and p_7 , *i.e.*, the participations of the GBT deformation modes **5** (symmetric distortion) and **7** (web-triggered local) on the column (distortional) critical buckling modes – recall that these modal participations were shown to exhibit some correlation with the b_w/b_f ratio. The observation of these results prompts the following remarks:

- (i) Although there is a considerable scatter of the P_{10t}/P_{cr} values for all the combinations of cross-section shape and GBT modal participation considered. However, the least of such scatters clearly concerns the lipped channel columns and local mode participations (p_7) – moreover, the corresponding P_{10t}/P_{cr} vs. p_7 plot shows that the presence of the local mode **7** entails a visible column post-critical

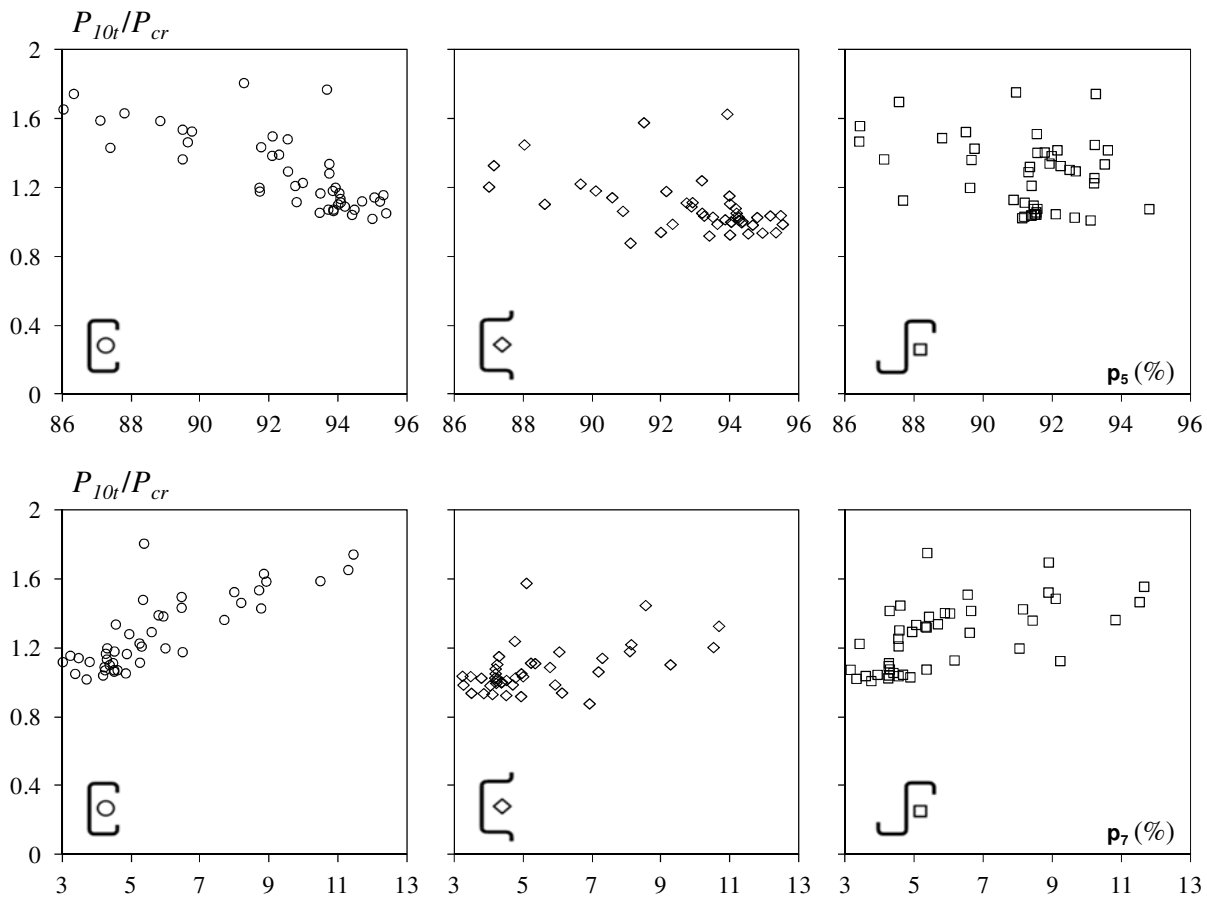


Figure 10: Variation of P_{10t}/P_{cr} with the GBT modal participations p_5 and p_7 (in the column critical buckling mode)

- strength increase (which is logical). The same does not occur for the hat-section and zed-section columns, which exhibit more scattered P_{10t}/P_{cr} values – nevertheless, the upward trend is still there.
- (ii) Naturally, the trends of the P_{10t}/P_{cr} vs. p_5 plots are practically the “inverse” of those exhibited by their P_{10t}/P_{cr} vs. p_7 counterparts, which means that now an increase in the participation of mode 5 causes a column post-critical strength drop (downward trend). Quantitatively speaking, the scatter of the P_{10t}/P_{cr} values is either (ii₁) very similar to that observed for the variation with p_7 (Hs and Zs) or (ii₂) slightly above it (Cs) – in any case, the lipped channel column results still exhibit the lower scatter.
 - (iii) It may be safely argued that the modal participations p_5 and p_7 provide fairly good indicators of the lipped channel column post-critical strength level (p_7 slightly outperforms p_5). No such claim can be safely made for hat-section and zed-section columns, even if a qualitatively similar trend is followed.

5. Concluding Remarks

This paper reported the available results of a numerical research effort currently under way that aims at assessing and mechanically interpreting the influence of the cross-section geometry and end support conditions on the elastic distortional post-buckling behavior and strength of cold-formed steel columns. This work dealt exclusively with simply supported (pinned end sections that can warp freely) columns with lipped channel, hat and zed cross-sections, which share common critical distortional buckling loads – *i.e.*, the columns eligible for this investigation were grouped in various column triplets. Initially, the paper addressed the column geometry selection (cross-section dimensions and lengths), carried out by means sequences of “trial-and-error” GBT-based buckling analyses, which led to the identification of 44 column triplets (i) buckling in “pure” distortional modes and (ii) deliberately exhibiting a wide range of cross-section proportions. While performing the buckling analyses, and taking advantage of the GBT unique modal decomposition features, the various column critical buckling modes were also mechanically characterized – their most relevant modal participations were identified and quantified, thus providing invaluable knowledge that helps in predicting the column post-buckling behavior and strength. Then, the paper presented and discusses the elastic post-critical strength of the selected column triplets, obtained from geometrically non-linear shell finite element analyses performed in the commercial code ANSYS – a representative sample of the corresponding equilibrium paths and post-buckling deformed configurations were also shown for illustrative purposes. In particular, the collected post-critical strength data bank was used to attempt identifying key parameters (*e.g.*, cross-section dimension ratios or critical buckling mode mechanical characteristics, *i.e.*, deformation mode participations), in the sense that they play a pivotal role in influencing the features exhibited by the column distortional post-buckling behavior, namely its post-critical strength – these parameters will certainly have relevant impact on the development of an efficient (safe and accurate) design approach for columns (i) exhibiting arbitrary cross-sections and support conditions, and (ii) failing in distortional modes.

Regardless of the cross-section shape, it was found that, in fact, the so-called “pure distortional buckling modes” exhibit not only anti-symmetric distortional deformations (the predominant ones), but also web-triggered local deformations – moreover, the relative contribution of these deformations depends on the column cross-section shape and dimensions in a non-negligible fashion. It was found that, generally, an increase in the presence of local deformations in the column critical (distortional) buckling mode leads to a higher post-critical strength (which seems logical, in view of the high post-critical strength reserve associated with local buckling). Finally, it was also found that more significant local deformations occur in columns exhibiting large web-to-flange width ratios, which is perfectly in line with the well known higher vulnerability of wider webs to local buckling effects.

Concerning the correlation of the column post-critical strength with its cross-section dimension ratios and buckling mode GBT modal participations, it was found that, in the case of lipped channel columns, the variations of the (i) web-to-flange width ratio and (ii) percentage participation of the web-triggered local mode 7 provide the reasonable well the means to predict the post-critical strength change. No similar trait could be found for the hat-section and zed-section columns, for which the above correlation is visibly weaker (even if qualitatively similar). Although these preliminary findings are quite encouraging, it is undeniable that considerable further research is required before more solid conclusions can be drawn.

Finally, it is worth mentioning that the authors plan to complement the investigation reported in this paper with the performance of GBT-based elastic post-buckling analyses of several columns – the modal features of such analyses (*e.g.*, Silvestre & Camotim 2003, 2006 or Basaglia *et al.* 2011) will definitely shed new light on the mechanics underlying the column distortional post-buckling behavior and on their dependence of the cross-section shape and dimensions. Moreover, it also planned to extend the scope of this investigation to (i) simply supported columns with more complex cross-sections, namely those exhibiting intermediate web and/or flange stiffeners, and (ii) columns with other end support conditions. Hopefully, the outcome of this research effort will contribute to improve the current knowledge on the column distortional mechanics, thus paving the way for the development of an improved DSM-based design approach for cold-formed steel columns failing in distortional modes.

References

- ABNT (2010). *Brazilian Standard on Design of Cold-Formed Steel Structures* (ABNT NBR 14762:2010), Brazilian Standards Association, Rio de Janeiro, RJ. (Portuguese)
- AS/NZS (2005). *Cold-Formed Steel Structures*, Standards of Australia (SA) and Standards of New Zealand (SNZ), Sydney-Wellington.
- Basaglia C, Camotim D, Silvestre N (2011). “Non-linear GBT formulation for open-section thin-walled members with arbitrary support conditions. *Computers and Structures*, **89**(21-22), 1906-1919.
- Bebiano R, Pina P, Silvestre N, Camotim D (2008a). *GBTUL 1.0 β – Buckling and Vibration Analysis of Thin-Walled Members*, DECivil/IST, Technical University of Lisbon. (<http://www.civil.ist.utl.pt/gbt>)
- Bebiano R, Silvestre N, Camotim D (2008b). “GBTUL – A code for the buckling analysis of cold-formed steel members”, *Proceedings of 19th International Specialty Conference on Recent Research and Developments in Cold-Formed Steel Design and Construction* (St. Louis, 14-15/10), R. LaBoube, W.W. Yu (eds.), 61-79.
- Camotim D, Silvestre N, Gonçalves R, Dinis PB (2004). “GBT analysis of thin-walled members: new formulations and applications”, *Thin-Walled Structures: Recent Advances and Future Trends in Thin-Walled Structures Technology*, J. Loughlan (ed.), Canopus Publishing Ltd., Bath, 137-168.
- Dinis PB, Camotim D, Silvestre N (2006). “GBT formulation to analyse the buckling behaviour of thin-walled members with arbitrarily ‘branched’ open cross-sections”, *Thin-Walled Structures*, **44**(1), 20-38.
- Dinis PB, Young B, Camotim D (2012), “Strength, failure and design of web-stiffened lipped channel columns exhibiting distortional buckling”, *Proceedings of Sixth International Conference on Coupled Instabilities in Metal Structures* (CIMS 2012 – Glasgow, 3-5/12), J. Loughlan, D. Nash, J. Rhodes (eds.), 531-538.
- Dinis PB, Camotim D (2013). “On the shell finite element buckling and post-buckling analysis of cold-formed steel members”, *submitted for publication*.
- Landesmann A, Camotim D (2010). “Distortional failure and design of cold-formed steel lipped channel columns under fire conditions”, *Proceedings of SSRC Annual Stability Conference* (Orlando, 12-15/5), 505-532.
- Landesmann A, Camotim D (2011). “DSM design of cold-formed steel columns against distortional failure: investigation on the influence of the cross-section geometry and support conditions”, *USB Key Drive Proceedings of Structural Stability Research Council Annual Stability Conference* (Pittsburgh, 10-14/5).
- Landesmann A, Camotim D (2013). On the direct strength method (DSM) design of cold-formed steel columns against distortional failure, *Thin-Walled Structures*, in press.

- NAS (2007). *North American Specification for the Design of Cold-Formed Steel Structural Members* (AISI-S100-07), American Iron and Steel Institute (AISI), Washington, DC.
- Prola LC, Camotim D (2002). "On the distortional post-buckling behavior of cold-formed lipped channel steel columns", *Proceedings of SSRC Annual Stability Conference* (Seattle, 24-27/4), 571-590.
- SAS (Swanson Analysis Systems Inc.) (2009). *ANSYS Reference Manual* (version 12).
- Schafer BW (2008). Review: the Direct Strength Method of cold-formed steel member design, *Journal of Constructional Steel Research*, **64**(7-8), 766-88.
- Silvestre N, Camotim D (2002a). "First order Generalised Beam Theory for arbitrary orthotropic materials", *Thin-Walled Structures*, **40**(9), 755-789.
- Silvestre N, Camotim D (2002b). "Second order Generalised Beam Theory for arbitrary orthotropic materials", *Thin-Walled Structures*, **40**(9), 791-820.
- Silvestre N, Camotim D (2003). "Non-linear Generalised Beam Theory for cold-formed steel members", *International Journal of Structural Stability and Dynamics*, **3**(4), 461-490.
- Silvestre N, Camotim D (2006). "Local-plate and distortional post-buckling behavior of cold-formed steel lipped channel columns with intermediate stiffeners", *Journal of Structural Engineering* (ASCE), **132**(4), 529-540.
- Yap DCY, Hancock GJ (2011). "Experimental study of high strength cold-formed stiffened web steel sections", *Journal of Structural Engineering* (ASCE), **137**(2), 162-72.